Response Characteristics of a Base-Isolated Structure Incorporated with a Force-Restricted Viscous Mass Damper

S. Nakaminami
Aseismic Device,CO.,LTD., Tokyo, Japan

K. Ikago & N. Inoue
Graduate School of Engineering, Tohoku University, Sendai, Japan

H. Kida
Aseismic Device,CO.,LTD., Tokyo, Japan

15 WCEE
LISBOA 2012

SUMMARY:
In this study, the application of a rotational viscous mass damper with a force-restriction mechanism to base-isolated structures and its effectiveness were evaluated. The force-restriction mechanism is represented by a complex-valued stiffness model, and the response characteristic of this system is based on the equivalent linearization method. The effectiveness of this system is examined by nonlinear time history response analyses, and the results confirmed the possibility of applying large additional masses to base-isolated structures. In addition, a large displacement reduction effect is achieved by using the force-restriction mechanism, which clearly indicates that damping force can be controlled. Finally, a practical design method for a base-isolated multistory structure incorporated with a force-restricted viscous mass damper is discussed.

Keywords: Rotary inertia mass, Base-isolated structures, Damper force restriction, Viscous mass damper, Multistory model

1. INTRODUCTION

It is known that configuring a secondary mass activated by relative acceleration in parallel to primary stiffness produces an elongated natural period and reduces input excitation, thereby decreasing the response displacement of the upper structure of a base-isolated building (Furuhashi and Ishimaru 2004, Furuhashi and Ishimaru 2006). Although a larger effective mass yields a better response reduction effect, such a mass may result in the generation of excessive damper reaction force. This is because the secondary mass sensitively responds to input relative acceleration. Therefore, we propose a force-restriction mechanism using rotary friction to avoid generation of excessive reaction force (Kida *et al*. 2011, Sumiyama *et al*. 2010, Isoda *et al*. 2010).

A force-restricted viscous mass damper (FRVMD) (Kida *et al*. 2011) is a device that limits the resultant of viscous and inertial forces generated by the damper. Substantial energy dissipation is also achieved by the force-restriction mechanism. A very large apparent mass, which is nearly equal to that of the primary mass, can be easily obtained using a ball screw amplifying mechanism and a cylindrical flywheel with a very small actual mass. Effective reductions in acceleration and damper reaction force without deterioration in the effects of natural period elongation and input reduction by the addition of a secondary mass can be achieved by the intentional use of the energy dissipation in the force-restriction mechanism and an optimally designed damper limit force.

In this study, we discuss the applicability of this device to a base-isolated structure (Nakaminami *et al*. 2011). First, a base-isolated structure incorporated with the FRVMD as a nonlinear system is modeled as an equivalent linear system. As in the linearization technique (Ikago *et al*. 2010), the hysteresis characteristics of the force-restriction mechanism are represented by complex-valued stiffness, where the generated reaction force is independent of the exciting frequency. Second, steady-state solutions are obtained from the equivalent linear system, and the transfer characteristics in the frequency domain and the effect of the force-restriction mechanism are elucidated by harmonic analyses. Finally, a practical design method of a base-isolated multistory structure incorporated with the FRVMD is discussed.

2. OUTLINE OF THE FORCE-RESTRICTED VISCOUS MASS DAMPER

A schematic representation of the FRVMD is shown in Figure 1; the analytical models and hysteresis characteristics of each element are shown in Figure 2.

An FRVMD is a device with an amplifying mechanism in which a ball screw converts linear motion into high-speed rotational motion. The amplified motion in the rotational direction yields viscous damping and inertial forces generated by the viscous fluid (silicone oil) and cylindrical flywheel, respectively. The forces in the rotational direction are amplified further when they are converted back to the translational direction by the ball screw mechanism. The apparent translational mass effect of the cylindrical flywheel, which is represented by m_d, is also amplified by the ball screw mechanism.

The resultant of the viscous damping and inertial forces in the rotational direction are transmitted to the ball nut through the friction material inserted between the cylindrical flywheel and ball nut. When the traction between these two components breaks, the damper axial force is restricted. The limit force of the damper can be adjusted by the axial forces introduced into the coned disk springs that hold the friction material.

In the analytical model shown in Figure 2, a friction element with a maximum friction of F_r is arranged in series with the supporting spring element having a stiffness of k_b. These elements are also connected to the viscous mass damper, which consists of the viscous element with a damping coefficient of c_d and a rotational mass element with an apparent translational mass of m_d in a parallel configuration.

The specifications of the FRVMD used in the analytical example are shown in Table 1. Provided that the ball screw lead is 40 mm and the diameter and length of the cylindrical flywheel are 600 mm and 1,700 mm, respectively, the translational apparent mass of the cylindrical flywheel, whose actual mass is 1.5 mt, is amplified 2,000 times. Thus, the device obtains a translational apparent mass effect of 3,000 mt.

A damping force of 1,000 kN is generated when the device is subjected to an axial velocity of 1.5 m/s, provided that the length of the internal and external cylinders is 1,000 mm, the gap between the cylinders is 2 mm, and the viscosity of the silicone oil enclosed between the cylinders is 10,000 cSt.

An arbitrary restriction force ranging from 1,500 kN is yielded by adjusting the axial force applied to the eight coned disk springs circumferentially placed on the cylindrical flywheel.

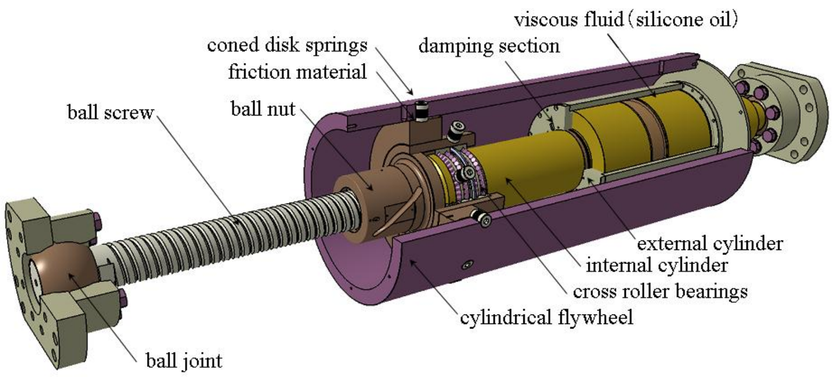

Figure 1. Schematic representation of the force-restricted viscous mass damper

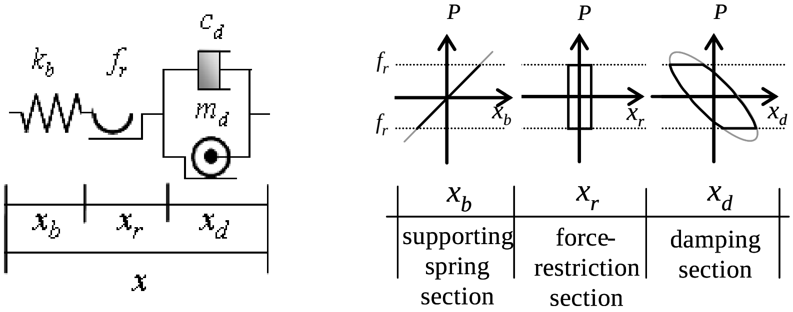

Figure 2. Analysis models and hysteresis characteristics of each element

Table 1. Specifications of the force-restricted viscous mass damper

amplification section		diameter of the ball screw	D_B	120	(mm)
		Lead Length of the ball screw	L_d	40	(mm)
damping section	rotational mass element	diameter of the cylinderical flywheel	D_o	600	(mm)
		length of the the cylinderical flywheel	L_o	1,700	(mm)
		amplification ratio of mass	β	2,000	
		equivalent mass	m_d	3,000	(ton)
	viscous element	diameter of the internal cylinder	D_i	219.4	(mm)
		length of the internal cylinder	L_e	1,000	(mm)
		gap between the internal and external cylinder	d_y	2.0	(mm)
		viscosity	η_{25}	100,000	(cSt)
		amplification ratio of velocity	S	17.2	
		viscous damping force (at 1.5m/s)	Q_v	1,000	(kN)
force-restriction section		restriction force	F_r	1,500	(kN)

3. TRANSFER CHARACTERISTICS OF A BASE-ISOLATED SYSTEM WITH THE FRVMD

3.1. Equivalent Linearization of the FRVMD

As stated previously, the hysteresis loop of the force-restriction element can be expressed as a rigid-plastic hysteresis. Therefore, an equivalent linearization is required to discuss the transfer characteristics of a base-isolated structure incorporated with an FRVMD.

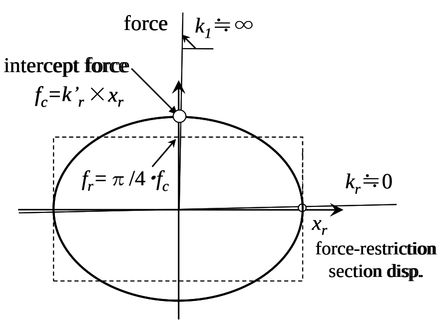

Figure 3. Equivalent linearization of friction element

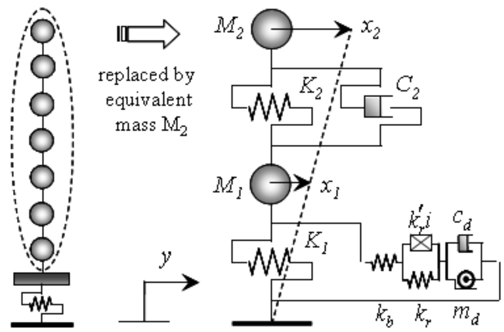

Figure 4. Equivalent two-degree-of-freedom model

Figure 3 shows the mechanism by which the hysteresis of the friction element is linearized. The rate-independent damping described by the complex stiffness is used to express the characteristics of the force-restriction element. The loss stiffness k_r' is determined such that the energy per cycle dissipated by the rate-independent damping model is equivalent to that of the rigid-plastic hysteresis model.

Because a two-degree-of-freedom model has the same minimum degree of freedom as a multi-degree-of-freedom (MDOF) model, for simplicity, the MDOF upper structure is reduced to a two-degree-of-freedom model (Figure 4).

3.2. Equations of motion and transfer function

The equations of motion for the FRVMD system are described as follows:

$$\begin{cases} M_2\ddot{x}_2 + C_2(\dot{x}_2 - \dot{x}_1) + K_2(x_2 - x_1) = -M_2\ddot{y} \\ M_1\ddot{x}_1 - C_2(\dot{x}_2 - \dot{x}_1) + K_1x_1 - K_2(x_2 - x_1) + f_d = -M_1\ddot{y} \\ y = x_1 + x_2 \end{cases} \tag{3.1}$$

$$f_d = \frac{k_b(k_r + k'_r i)(-m_d p^2 + ic_d p)}{(k_b + k_r + k'_r i)(-m_d p^2 + ic_d p) + k_b(k_r + k'_r i)} x_1 = F_D(ip)x_1 \tag{3.2}$$

where f_d is the damping force; M_i, K_i, and C_i are the mass, stiffness, and damping coefficient of the ith story of the primary structure, respectively; k_b, c_d, and m_d are the stiffness of the damper supporting the spring, damping coefficient, and equivalent translational mass of the FRVMD, respectively; x_b, x_d, and x_r are the displacements of the supporting spring, viscous mass damper, and the slip displacement of the force-restriction mechanism, respectively; finally, y and p are ground displacement and exciting frequency, respectively.

The displacement of the isolation layer x_1 and that of the superstructure x_2 is expressed as $x_1(t) = X_1e^{ipt}$ and $x_2(t) = X_2e^{ipt}$ when the primary system is subjected to harmonic ground motion $y(t) = Ye^{ipt}$. Substituting $x_1(t) = X_1e^{ipt}$, $x_2(t) = X_2e^{ipt}$, into Eq. (3.1) gives the following transfer functions:

$$H_{D1}(ip) = \frac{X_1}{\ddot{Y}} = \frac{1}{-p^2}\cdot\frac{X_1}{Y} = \frac{M_1p^2 - \dfrac{M_2p^2(K_2 + iC_2p)}{M_2p^2 - iC_2p - K_2}}{-M_1p^2 + K_1 + \left(\dfrac{K_2 + iC_2p}{M_2p^2 - iC_2p - K_2} + 1\right)(K_2 + iC_2p) + F_D(ip)} \times \frac{1}{-p^2} \tag{3.3}$$

$$H_{D2}(ip) = \frac{X_2}{\ddot{Y}} = \frac{1}{-p^2}\cdot\frac{X_2}{Y} = \frac{M_2p^2 + (K_2 + iC_2p)\dfrac{X_1}{Y}}{-M_2p^2 + iC_2p + K_2} \times \frac{1}{-p^2} \tag{3.4}$$

$$H_{A1}(ip) = \frac{X_1 + \ddot{Y}}{\ddot{Y}} = \frac{X_1}{Y} + 1 \tag{3.5}$$

$$H_{A2}(ip) = \frac{X_2 + \ddot{Y}}{\ddot{Y}} = \frac{X_2}{Y} + 1 \tag{3.6}$$

3.3. Effects of force restriction and filter spring

In this section, we discuss the damping effect of force restriction and the filtering effect of the supporting spring using the transfer function derived in the previous section in order to understand the transfer characteristics of the MDOF base-isolated structure incorporated with the FRVMD. The eight-degree-of-freedom superstructure shown in Table II is reduced to an equivalent two-degree-of-freedom model. The base-isolation system is designed such that the natural period T_1 is 4 s without the damper. We assume that the inherent damping h of the primary structure is 2% of the critical damping when the base is fixed. The inherent damping of the base-isolation layer is ignored. The damper is designed such that the secondary mass ratio μ = 1.0, additional damping ratio h_d = 20% of the critical damping of the base-isolation system, and the natural frequency of the filter spring γ_d = 4.0 Hz.

The specifications of the analytical model are shown in Table 2. A parametric survey was conducted in which the loss stiffness k'_r was varied. If the loss stiffness k'_r is infinity, the damper represents a force-unrestricted viscous mass damper because slip displacement never occurs in the friction element. In the numerical study, a large value, 10^{10}, instead of infinity is used as k'_r. In cases of FR1, FR2, FR3, and FR4, the values 10^8, 3E10^7, 2.1E10^4, and 10^3 are used as k'_r, respectively. A fixed point exists on the resonance curve, regardless of the loss stiffness k'_r. An optimum k'_r to minimize the resonance curve peak is sought such that the resonance curve has an extreme value at the fixed point. In this study, case FR3 exhibits optimum loss stiffness. Case VD is also compared, in which the damper is a viscous damper ($k'_r = \infty$, $\mu = 0$) with a damping ratio of 20% of critical damping.

Table 2. Specifications of the analytical model

story	eight-degree-of-freedom model			two-degree-of-freedom model		
	height(m)	mass(ton)	stiffness(kN/m)	height(m)	mass(ton)	stiffness(kN/m)
i	Hi	mi	ki	Hi	mi	ki
7	4.70	1,039	1,475,900			
6	3.80	3,897	3,143,400			
5	3.80	3,477	4,581,300			
4	3.80	3,600	4,976,600	4.14	21,015	1,195,770
3	4.40	3,615	3,877,500			
2	4.40	3,856	4,075,700			
1	5.45	4,671	3,519,300			
isolation layer	0.10	6,115	66,940	0.10	6,115	66,940
total	30.45	30,269	-	4.2	27,130	-

Resonance curves of cases VD, VMD, and FRVMD (FR1–FR4) are shown in Figure 5. T_1 represents the natural period of the primary structure without the damper. T'_1 and T_2 are the first and second natural periods, respectively, of the system with the secondary mass. T_d is the natural period of the filter spring.

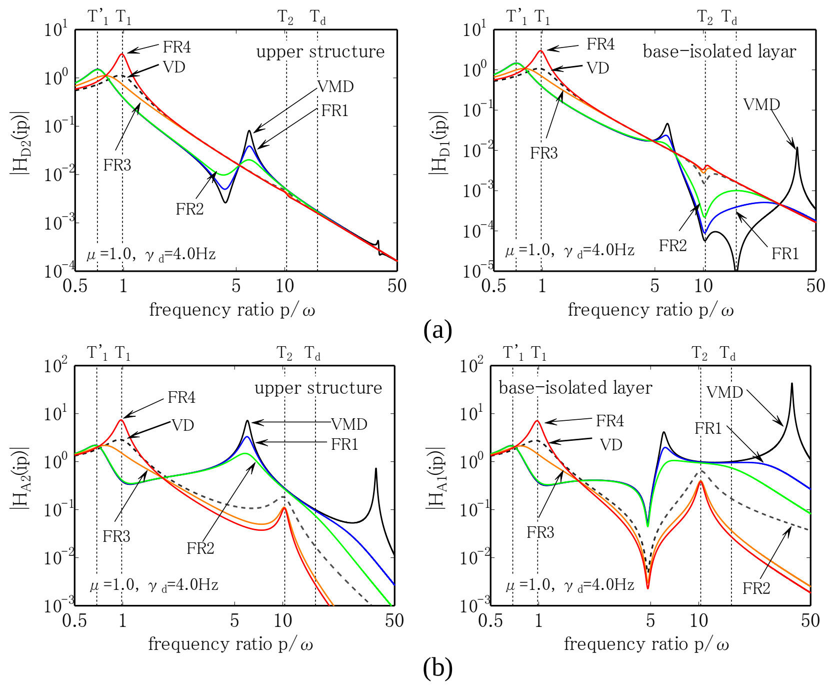

Figure 5. Effect of (a) force-restriction displacement and (b) factor acceleration amplification factors

In cases VMD, FR1, FR2, and FR3, the period elongation effect of the secondary mass shifts the peak amplification factor of the first mode from T_1 to T'_1. Although the peak value of the displacement amplification factor around period T_2 varies with the loss stiffness k'_r, the maximum displacement may be nearly unaffected by loss stiffness because the peak value itself is very small. Figure 5 (a) shows that the maximum value of the displacement amplification factor decreases as the loss factor k'_r decreases from infinity (VMD) to the optimum value (FR3). As the loss factor decreases from the optimum value, the frequency of the maximum amplification factor increases up to T_1. On the other hand, the higher frequency components of the displacement amplification factors are considered to have little effect on the maximum response displacement, as indicated in Figure 5 (b). In contrast, the higher frequency components of the acceleration amplitude factors have the largest effect on maximum response acceleration.

In previous studies, the natural frequency of the filter spring was fixed at 4.0 Hz. Here, we study the response of the filter spring by varying frequency. The mass ratio μ, damping factor h_d, and loss stiffness k'_r are fixed at 1.0, 0.2, and 10^{10} (to represent infinity), respectively, and the filter spring frequency γ_d is varied from 4.0 Hz to 0.5 Hz. Figure 6 shows the effects of filter spring frequency on amplitude factors.

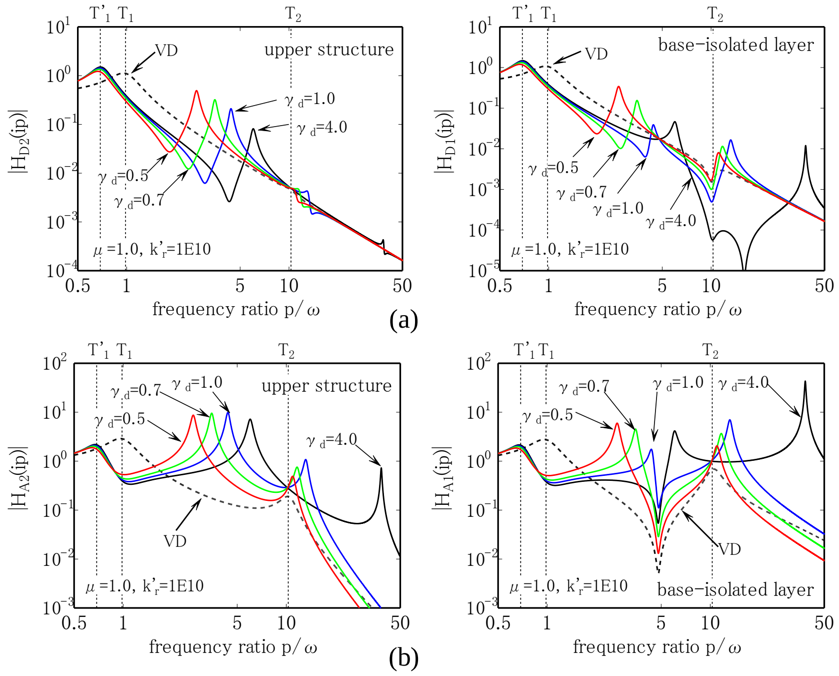

Figure 6. Effects of filter spring frequency on resonance curves:
(a) displacement amplification factors, (b) acceleration amplification factors

As shown in Figure 6, the resonance curves have peaks at frequencies near the frequency ratio p/ω = 50 only in the case of γ_d = 4.0 Hz. These peaks are considered to cause the very large response acceleration in the upper structure because input ground motions generally contain many high-frequency components. This peak in the high-frequency range is considered to occur only when filter spring frequency is close to the second natural frequency of the primary system. Decreasing filter spring frequency (γ_d = 1.0, 0.7, and 0.5 Hz) avoids the occurrence of peaks in the high-frequency range, as shown in the figure. In addition, varying filter spring frequency seldom changes the maximum value of the displacement amplitude factor. This finding suggests that choosing an appropriate filter spring frequency will enable reducing the maximum response acceleration of the upper structure without deterioration of the maximum response displacement.

Thus, it is expected that period elongation and filter spring effects ensure that the FRVMD controls seismic response displacement more effectively than a conventional viscous damper without deterioration in acceleration response.

4. RESPONSE ANALYSIS IN THE TIME DOMAIN

In this section, we confirm the advantage of the FRVMD incorporated into a base-isolated building subjected to seismic ground motions by conducting nonlinear time history analyses. The same analytical model as in the previous study is used and is subjected to the NS component of the El Centro records of the 1940 Imperial Valley earthquake scaled by 150% and the EW component of an artificial ground motion (hereinafter referred to as the Sannomaru ground motion) that simulates the ground motion caused by the hypothetical Tokai-Tonankai earthquake in Nagoya City, Japan. The Sannomaru ground motion is a ground motion to which base-isolated structures are vulnerable because it has long duration and many components resonating with the base-isolation period.

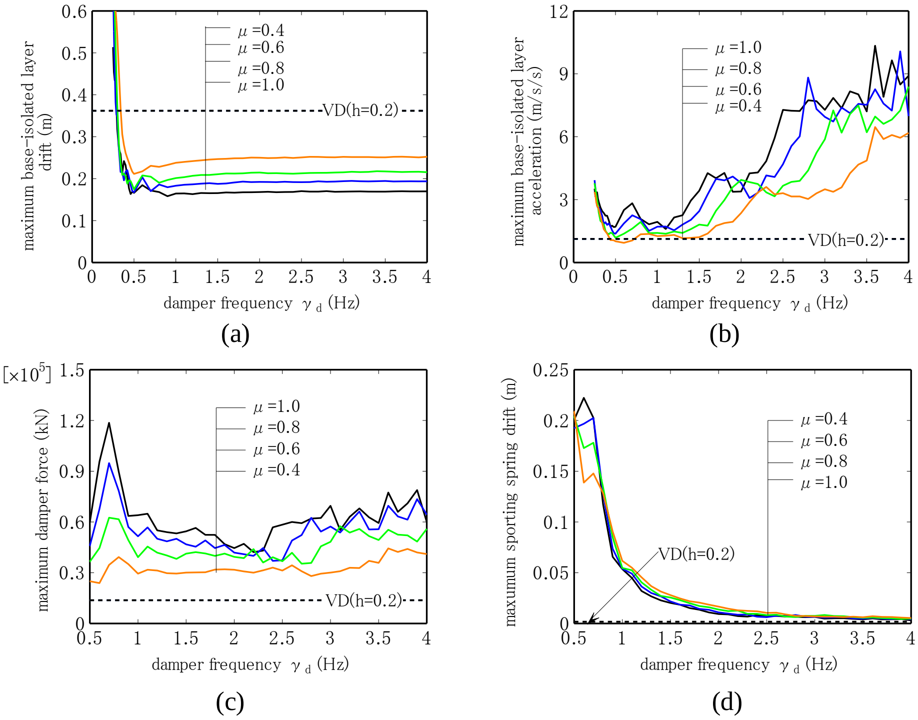

Figure 7. Relationship between maximum response value and filter spring frequency (force unrestricted): (a) displacement amplification factors, (b) maximum upper story acceleration, (c) maximum damper force, (d) maximum supporting spring drift

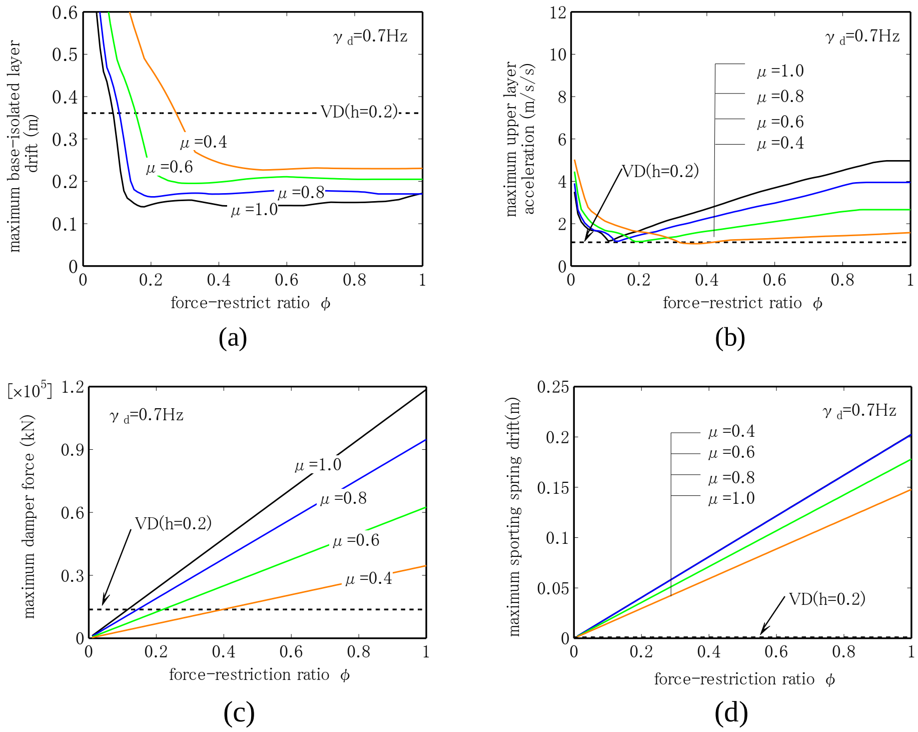

Figure 8. Relationship between maximum response value and force-restriction ratio: (a) maximum base-isolated story drift, (b) maximum upper story acceleration, (c) maximum damper force, (d) maximum supporting spring drift

Here, we define the force restriction ratio ϕ as the ratio of the restriction force to the response reaction force generated when the damper force is unrestricted. Figure 7 shows the relationship between the filter spring frequency and the maximum responses obtained by the nonlinear time history analyses of the base-isolated building incorporated with the FRVMD and subjected to Sannomaru ground motion, in which the damper force is unrestricted, i.e., ϕ equals 1. On the other hand, the response deformations of the base-isolation layer are kept smaller than that in case VD. When the filter spring frequency is greater than 0.5 Hz, the maximum response accelerations decrease to the same value obtained by the system with VD as the filter spring frequency decreases to 0.5 Hz. In addition, deformation of the supporting spring decreases as the filter spring frequency increases.

Figure 8 shows the relationship between the force-restriction ratio and the maximum responses with a filter spring frequency of 0.7 Hz, which was determined using Figure 7 to be the best frequency for Sannomaru ground motion. As shown in Figure 8, the force-restriction mechanism achieves reduction in the maximum acceleration and reaction damping force without the deterioration of maximum displacement if the force-restriction ratio is properly determined.

Thus, the advantage of applying the filter spring to the FRVMD shown in the frequency domain analyses is also confirmed by time domain analyses.

5. DESIGN EXAMPLES

5.2. Analytical models

This section shows design examples of an eight-story reinforced concrete building using six cases: (i) no dampers and (ii) four types of dampers. The specifications of the upper structure and the layout of isolators are shown in Table 3 and Figure 9, respectively.

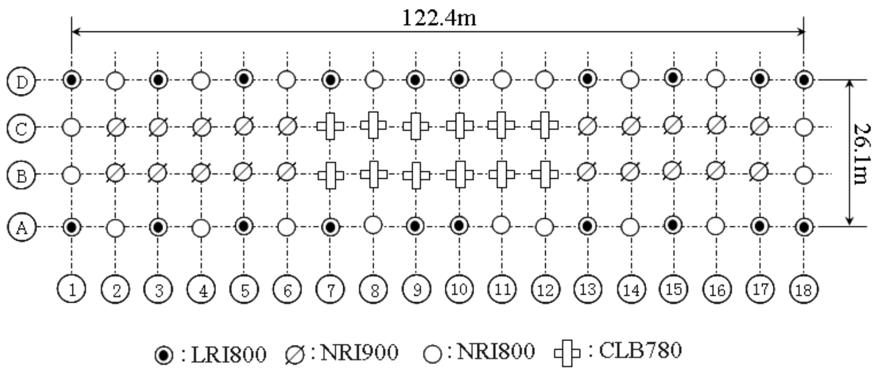

Figure 9. Layout of isolators (VD model)

Table 3. Specifications of the all properties of the FRVMDs

damping coefficient	C_1	171,616	(kN・s/m)
Nonlinear factor	α	0.35	
force-restriction load	F_r	1,500	(kN)
viscous damping force	Q_v	1,000	(kN)
inertial force	Q_i	3,000	(kN/G)

The first example, hereinafter referred to as the UD model, is a base-isolated structure without dampers and has an equivalent natural period of 4 s when the maximum response displacement is 0.4 m. The second example, hereinafter referred to as the VD model, has the same natural period as that of the UD model and is incorporated with viscous dampers. The third example, hereinafter referred to as the FRVMD model, has an equivalent natural period of 3.6 s when the maximum response displacement is

0.4 m and is incorporated with FRVMDs. The fourth and fifth examples have the same natural period as that of the FRVMD model and are incorporated with a viscous mass damper (hereinafter referred to as the VMD model) and a viscous mass damper connected with a filter spring (hereinafter referred to as the FVMD model), respectively.
The UD and VD models are equipped with 40 natural rubber isolators (NRIs), 20 lead rubber isolators (LRIs), and 12 cross-linear bearings (CLBs), as shown in Figure 9. The NRIs and LRIs provide restoring forces, whereas the CLB provides no restoring force. The LRI is equipped with a lead plug and provides hysteretic damping. The natural period of the FRVMD, VMD, and FVMD models is shorter than that of the UD and VD models because all CLBs used in the UD and VD models are replaced by NRIs.

The total yield shear force provided by the lead plugs in the LRIs is approximately 2% of the upper structure weight. The El Centro NS record (PGV = 7.5 m/s) and Sannomaru ground motion are used as input ground motions. We assume that the hysteresis of the base-isolation layer is bilinear and that of the upper structure is linear. The inherent damping of the upper structure is assumed to be 2% of critical damping with its base fixed.

Specifications of the analytical model of the FRVMD are shown in Table III. Eight FRVMDs are incorporated into the FRVMD model. Each FRVMD has an apparent translational mass of 3,000 mt, generates a viscous damping force of 1,000 kN at a velocity of 1.5 m/s, and has a restriction force of 1,500 kN. The total apparent mass of the eight dampers equals 80% of the primary mass. The force restriction ratio is 20%. The stiffness of the supporting spring is designed such that the filter spring frequency γ_d equals 0.7 Hz. In addition, eight VDs are incorporated into the VD model for comparison.

Each VD is equipped with a relief valve that opens when the velocity reaches 0.32 m/s and a damping force of 800 kN is generated. After the relief valve opens, the damping coefficient of the damper is reduced so that the generated damping force is 1,000 kN at a velocity of 1.5 m/s.

5.2. Analytical results

The analytical results are shown in Figure 10. The filter spring in the FVMD reduced response acceleration without deterioration of response displacement, whereas the VMD model showed excessive acceleration in the upper structure. Furthermore, by equipping force restriction in the FRVMD model, the response acceleration observed in the FVMD model reduced to nearly the same as that in the VD model. The maximum response displacement of the FRVMD model was reduced to approximately 80% that of the VD model. These design examples illustrate that the secondary mass obtains an apparent long period without using cross-linear bearings to achieve reduction in seismic response. In addition, appropriate filter spring frequency and damping force restriction are essential for the present damper.

6. CONCLUSIONS

In this paper, we compared seismic responses of a base-isolated building with no damper and that equipped with four different types of dampers: VD, VMD, FVMD, and FRVMD.

The harmonic response characteristics of the base-isolation system incorporated with FRVMDs were examined by linearizing the hysteresis of the rotary friction mechanism using complex-valued stiffness. The secondary mass obtained the period elongation effect, and the filter spring obtained a reduction in response acceleration. Furthermore, the force-restriction mechanism was determined to be effective not only in the reduction of the maximum damping force but also in the compensation of the energy dissipation deteriorated by the force restriction in the viscous element.

The analytical examples based on nonlinear time history analyses validated the results obtained by the study in the frequency domain.

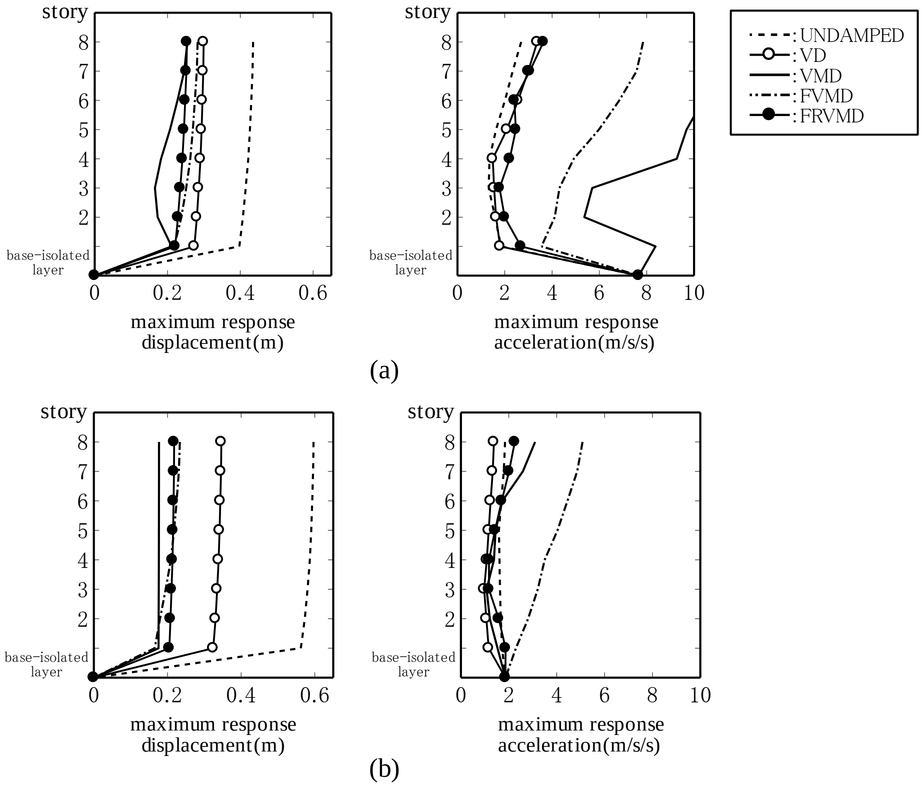

Figure 10. Maximum responses obtained through analytical results: (a) El centro-NS (75 kine), (b) Sannomaru

ACKNOWLEDGMENTS

This work was supported by a Grant-in-Aid for Scientific Research (B) No. 24360220 provided by the Japan Society for the Promotion of Science (JSPS) and a research grant provided by the Maeda engineering foundation.

REFERENCES

Furuhashi T., Ishimaru S. (2004). Mode Isolation By Inertial Mass Study on response control by inertial mass No.1. *Journal of Structural and Construction Engineering Architectural Institute of Japan*, No.576, 55-62. (in Japanese).

Furuhashi T., Ishimaru S. (2006). Response Control of Multi-Degree System By Inertial Mass Study on response control by inertial mass No.2. *Journal of Structural and Construction Engineering Architectural Institute of Japan*, No.601, 83-90. (in Japanese).

Ikago K., Inoue N. (2010). Seismic Displacement Control of Base-Isolated Structures using Complex Stiffness Model. *Journal of Structural and Construction Engineering Architectural Institute of Japan*, **Vol.75**, No.655, 1653-1660. (in Japanese).

Isoda K., Hanzawa T., Fukasawa T., Fukukita A. (2010). Development of Inertia Mass damper with Overload Prevention fuction, Part1: Purpose of Development and Summary of the Damper, Architectural Institute of Japan, 453-454. (in Japanese).

Kida H., Watanabe Y., Nakaminami S., Tanaka H., Sugimura Y., Saito K., Ikago K., Inoue N. (2011). Full-Scale Dynamic Tests of Tuned Viscous Mass Damper with Force Restriction Mechanism and Its Analytical Verification. *Journal of Structural and Construction Engineering Architectural Institute of Japan*, **Vol.76**, No.665, 1271-1280. (in Japanese).

Nakaminami S., Kida H., Ikago K., Inoue N. (2011). Application of Viscous Mass Damper with Force Restriction Mechanism to Base-Isolated Structure and Its Effectiveness. *Journal of Structural and Construction Engineering Architectural Institute of Japan*, **Vol.76**, No.670, 2077-2086. (in Japanese).

Sumiyama T., Arai T., Ikenaga M., Ikago K., Inoue N. (2010). A Study on a Seismic Vibration Control System using a Tuned Viscous Mass Damper, Part1: A Study on Effectiveness of a Damper Force Relief Mechanism, Architectural Institute of Japan, 449-450. (in Japanese).